Jet impingement heat transfer on a concave surface in a wing leading edge: experimental study and correlation development

Xueqin Bu[1] Long Peng[2] Guiping Lin[1] Lizhan Bai[1,3,*] Dongsheng Wen[3]

1 Laboratory of Fundamental Science on Ergonomics and Environmental Control, School of Aeronautic Science and Engineering, Beihang University, Beijing 100191, PR China

2 Institute of Engineering Thermophysics, Chinese Academy of Sciences, Beijing 100190, PR China

3 School of Chemical and Process Engineering, University of Leeds, Leeds, LS2 9JT, UK

Abstract: Extensive experimental studies of the heat transfer characteristics of jet impingement on a variable-curvature concave surface in a wing leading edge were conducted for aircraft anti-icing applications. The experiments were performed on a piccolo tube with three rows of aligned jet holes over a wide range of parameters: the jet Reynolds number (Re_j) from 50,000 to 90,000, the relative tube-to-surface distance (H/d) from 1.74 to 20.0, the jet impingement angle (α) from 66° to 90°, and the relative chordwise arc length in the jet impingement zone (r/d) from 13.2 to 34.8. The experimental results indicated that the heat transfer performance at the stagnation point was enhanced with increasing Re_j and α, and an optimal H/d existed to achieve the best heat transfer performance at the stagnation point. It was found that the attenuation coefficient curve of the jet impingement heat transfer in the chordwise direction exhibited an approximate bell shape with the peak located at the stagnation point, affected only by r/d in the peak zone. In the non-peak zone, however it was affected significantly by a variety of factors including Re_j, H/d and r/d. Experimental data-based correlations of the Nusselt number at the stagnation point and the distribution of the attenuation coefficient in the chordwise direction were developed and validated, which can be used to predict the performance of a wing leading edge anti-icing system.

Keywords: jet impingement; heat transfer; wing anti-icing; experiment; correlation

* Corresponding author. Tel.: +86 10 8233 8600; Fax: +86 10 8233 8600

E-mail address: bailizhan@buaa.edu.cn (L. Bai)

1 Introduction

Jet impingement promises excellent heat transfer performance, which has attracted worldwide interests for decades. As an effective measure to enhance the local heat transfer coefficient, it has been applied in a wide variety of fields, such as glass tempering, metal annealing, food and paper drying, and gas turbine blade and electronics cooling [1-5]. Because jet impingement is a very complex heat and mass transfer process, which is influenced by many parameters such as the shape and size of the nozzle, the nozzle layout, the nozzle to target surface distance, the jet Reynolds number, the impingement angle and the curvature of impinging surface, comprehensive experimental and theoretical studies have been conducted especially for jet impingement on a flat or cylindrical surface [6-13].

In aeronautical engineering, anti-icing or de-icing system is generally used in both civil and military aircraft to guarantee flight safety. The wing leading edge hot-air anti-icing system (WHAAIS) has been widely employed so far, where jet impingement heat transfer of hot air introduced from the engine compressor and sprayed from the jet holes on a piccolo tube is utilized to prevent the occurrence of icing on the external surface of a wing leading edge, as shown schematically in Fig. 1 [14]. Fig. 2 shows the schematic of the jet impingement on a variable-curvature concave surface in a wing leading edge hot air anti-icing system. Comparing to the common jet impingement on a flat surface, there are some notable differences in a WHAAIS as summarized below: 1) the pressure of the hot air supplied is usually very high, and the air in the jet holes is in the choked state with the outlet velocity reaching the speed of sound; 2) the jet hole profile is very sharp, and the air at the outlet of the jet holes may be still under expansion; 3) the piccolo tube usually has a single one, two or three rows of jet holes, and the circumferential angle of jet holes on the piccolo tube can significantly affect the fluid flow and heat transfer processes on the target surface; and 4) for piccolo tube with two or three rows of jet holes, the interaction of jets between adjacent holes further increases the complexity. The jet impingement in a WHAAIS is also much more complicated than

that on a cylindrical concave surface due to its continuous variable curvature character in the leading edge.

For the jet impingement heat transfer in a WHAAIS, only very limited experimental and theoretical studies has been reported to date. Jusionis [15] reported perhaps the first experimental study of jet impingement heat transfer on an enclosed surface in 1970. A piccolo tube with a single one row of jet holes was used in his study, and the correlation of the average heat transfer coefficient over the target surface was obtained considering the influences of the jet Reynolds number, the distance from the jet holes to the target surface and the circumferential angle of the jet holes on the piccolo tube. Brown et al. [16] investigated the performance of a piccolo tube with three rows of jet holes, and developed a correction of the average convective heat transfer coefficient on the jet impingement region, where the distance between the jet holes and the jet Reynolds number were considered. The review from Wright [17] suggested that Goldstein correlation [18] could be used for a first order estimation on the piccolo tube performance

In 2003, by using the computational fluid dynamics (CFD) method, Fregeau, Saeed and Paraschivoiu [19] studied the thermal performance of a 3-D hot air jet flow impinging on a normal semicircular concave surface instead of the leading edge of an aircraft wing. The correlations of the average and stagnation Nusselt number were obtained. In their study, only the layout of single one row of jet holes was considered. The average Nusselt number was found to be remarkably dependent on the tube-to-surface distance. The maximum Nusselt number occurred at the jet stagnation point, and the distance between adjacent jet holes had negligible effect on it. In 2008, Saeed [20] conducted a simulation study to further understand the jet impingement heat transfer performance employing a piccolo tube with single one row and two rows of staggered jet holes impinging on the internal surfaces of a typical aircraft wing/slat. The 3-D distributions of the Nusselt number and heat transfer coefficient on the target surface were illustrated, and the results showed that the jet impingement heat transfer performance for the piccolo tube with single one row and two rows of 20 degree staggered jet holes was better than that with

two rows of 10 degree staggered jet holes. In 2009, Fregeau, Paraschivoiu and Saeed [21] simplified the single one row of jet holes as one-quarter of the jet to reduce the size of computational domain, and the simulation results indicated that the local Nusselt number distribution on the surface was enhanced with the decrease of the tube-to-surface distance and increase of jet Mach number and the distance between adjacent jet holes.

In 2006, Papadakis and Wong et al. [22-24] performed an extensive parametric study to investigate the influence of tube-to-surface distance, jet hole location, the diffuser geometry, hot air temperature and mass flow rate on the jet impingement heat transfer performance of a bleed air ice-protection system by both experimental and numerical methods. The impinging surface simulated the NACA 23012 airfoil leading edge shape, and three rows of aligned jet holes were manufactured on the piccolo tube in this study. It was found that once the air flow in the jet holes was choked, air supply mass flux would have less influence on the anti-icing surface temperature than that of the supplied air temperature, and the tube-to-surface distance and the jet hole locations on the piccolo tube were critical in affecting the impinging surface temperature, however, the anti-icing cavity shape only exhibited very small effect. The system performance variation trends in the chordwise direction as a function of relevant parameters were also qualitatively presented.

Recently Imbriale and Ianiro et al. [25] reported the detailed temperature and heat flux distribution of a wing leading edge upon impingement from a single row of jets by using the IR thermography and the heated thin foil heat transfer sensor. The presence of streamwise vortices was observed, which was considered to be influenced by the surface curvature, jet hole spacing and jet impingement angle, and an average Nusselt number correlation was proposed based on the Meola's correlation [26] for jet impingement on a flat surface. The authors have recently reported an extensive experimental investigation of the jet impingement heat transfer characteristics on a variable-curvature concave surface in a wing leading edge [27]. In the experiments, different jet hole layouts were considered, and the relevant parameters such as the jet Reynolds number, tube-to-surface distance and

circumferential angle of jet holes on the piccolo tube were varied over a wide range. An optimal relative tube-to-surface distance of 4.5 under $Re_j = 51021$ was determined for the jet impingement with a single one row of jet holes. It was observed that the Nu_x curves exhibited much different shapes for jet impingement with two and three rows of aligned jet holes on the piccolo tube due to different intensities of interference between adjacent air jets.

As briefly reviewed above, different jet impingement heat transfer correlations have been proposed mainly for one row of jet holes, and the studies on impingement from two or three rows of jet holes on a piccolo tube are still less established. For practical applications, jets from multiple holes are more effective for anti-icing applications due to the increased heat transfer area in the wing leading edge. This paper reported an extensive experimental study of the heat transfer characteristics of jet impingement on a variable-curvature concave surface in a wing leading edge with three rows of aligned jet holes. A parametric study of the effects of the jet Reynolds number, the relative tube-to-surface distance, the jet impingement angle and the relative chordwise arc length in the jet impingement zone on the jet impingement heat transfer was conducted. Experimental data-based correlation equations at the stagnation point and the attenuation coefficient distribution in the chordwise direction were developed to advance our understanding on the design of a WHAAIS.

2 Experimental Setup

The experimental rig was the same as that in our previous paper [27], and only a brief introduction is provided here. The experimental system was composed of an air supply system, a test unit including an anti-icing cavity and piccolo tubes with three rows of aligned jet holes, a heating system and a data acquisition system. Interested readers can find detailed information in Ref. [27].

In order to minimize the heat loss to the ambience, rubber sponge insulation material with the thickness of about 10 cm were employed to cover the thin film heater, and the heat loss was estimated to be within 2.40%,

which can be safely neglected. Type T thermocouple junctions were placed in the blind holes with a depth of 2.5mm in the outer surface and fixed by adhesives with good heat conduction and electrical insulation. Because all the thermocouple wires were arranged outside the anti-icing cavity, the flow field in the cavity was not affected. The thermocouple junctions were located only 0.5 mm from the inner surface of the leading edge, which could represent the temperatures at the inner surface under the experimental conditions. The relevant parameter ranges in the experiments are listed in Table 1, where C_n is the spanwise distance between adjacent jet holes.

3 Data processing and uncertainty analysis

The inverse heat transfer method was adopted in the experiment, i.e., heat was transferred to the wing anti-icing cavity from the outside, just opposite to the actual situation. In order to investigate the flow and heat transfer in the wing anti-icing cavity, the outer surface of the leading edge of the anti-icing cavity was heated under a constant heat flux, and high pressure air with a fixed temperature of 300K was introduced into the cavity as a cooling medium.

Based on the experimental principle in this paper, the local convective heat transfer coefficient can be calculated as:

$$h_x = \frac{q}{T_{wx} - T_{in}} \tag{1}$$

where q is the heat flux at the outer surface of the leading edge; T_{wx} is the local temperature at the inner surface of the leading edge and T_{in} is the inlet temperature of the supplied air.

In equation (1), the air temperature at the inlet of the piccolo tube (T_{in}) should represent the total temperature of the air jet (because the air velocity in the piccolo tube is relatively small, the kinetic energy can be safely neglected, and the static temperature is very close to the total temperature). In this paper, we used the total temperature to calculate h and Nu directly, as shown in equation (1), and did not use the adiabatic wall temperature because it is rather difficult to measure directly without affecting the jet impingement flow field in

the anti-icing cavity in this experimental system. At the same time, for aircraft wing anti-icing applications, because the jet velocity is usually very large, i.e. at the sonic speed, and the tube-to-surface distance is not very long, i.e. < 40 mm, the effect of ambient heating to the air jet is very slight, and the calculated Nusselt numbers using the jet inlet temperature are acceptable for engineering design, as confirmed by our experimental results.

In addition, in the calculation of the local convective heat transfer coefficient, we did not take into account the tangential thermal conduction in the wall, so the results obtained here would slightly deviate from the actual ones to some extent. For practical applications as in this study, i.e., the anti-icing cavity model came from a real regional plane, this approach is preferable to guide the anti-icing cavity design without considering the tangential thermal conduction effect of the wall, which will make the design process more convenient.

The local Nusselt Number is expressed by equation (2):

$$\mathrm{Nu_x} = \frac{\mathrm{h_x d}}{\lambda} \tag{2}$$

where d is the diameter of the jet hole and λ is the thermal conductivity of air.

The jet Reynolds Number is defined by Equation (3):

$$\mathrm{Re_j} = \frac{\dfrac{\mathrm{G_m}}{\mathrm{N}\rho\pi\left(\mathrm{d}/2\right)^2}\mathrm{d}}{\nu} = \frac{4\mathrm{G_m}\times\mathrm{d}}{\rho\mathrm{N}\pi\mathrm{d}^2\left(\dfrac{\mu}{\rho}\right)} = \frac{4\mathrm{G_m}}{\mathrm{N}\pi\mathrm{d}\,\mu} \tag{3}$$

where $\mathrm{G_m}$ is the mass flowrate of air, N is the number of jet holes, ρ is the density of air, and μ and ν are the kinetic and dynamic viscosities, respectively.

In order to investigate the distribution characteristics of the local heat transfer performance in the chordwise direction of the leading edge, a new parameter that shows the ratio of the local Nussel number, $\mathrm{Nu_x}$, over the stagnation value, i.e. the attenuation coefficient ξ_x, is defined in Equation (4):

$$\xi_x = \mathrm{Nu_x} / \mathrm{Nu_{stag}} \times 100\% \tag{4}$$

Table 2 presents the measurement uncertainties of the directly measured parameters, such as the voltage,

resistance, temperature and flow rate. The uncertainties of h, Nu and ξ were calculated to be smaller than 5.0%.

4 Comparison and validation of the experimental results

To ensure the validity and reliability of the experimental results achieved in this work, a comparison with other available experimental data was attempted. However due to the difference in the geometry, it is very difficult to find an appropriate comparative case. The only similar example was from the work by Brown et al [16], who experimentally investigated a full-scale, 2-D model of an aircraft nacelle anti-icing system. The profile of the impingement surface as well as the operating conditions from Ref. [16] was quite similar to those in this work. Fig. 3 shows the comparison between our results and those from Brown et al. [16], where d = 1.5mm and H/d = 5, while in our experiment, d = 2mm and H/d = 6.63. As shown in Fig. 3, our experimental results for averaged Nusselt number exhibited a very similar trend with those from Brown et al.[16], with slightly smaller values caused by a higher relative tube-to-surface distance in our experiment. Such a comparison shows the reliability of the experimental results in this work.

5 Experimental Results and Discussions

Two aspects of the jet impingement heat transfer were considered in this part: the heat transfer performance at the stagnation point and the attenuation distribution characteristics in the chordwise direction. For the first aspect, the influences of the jet Reynolds number Re_j, the relative tube-to-surface distance H/d and the jet impingement angle α on the stagnation Nusselt number, Nu_{stag}, were studied; and for the second one, the influences of the Re_j, H/d and the relative chordwise arc length in the jet impingement zone r/d on the distribution characteristics of the attenuation coefficient ξ_x were investigated. Finally the correlations of the Nu_{stag} and ξ_x were acquired and experimentally validated.

5.1 Effects of jet Reynolds number and relative tube-to-surface distance on Nu_{stag}

Fig. 4 illustrates the influences of Re_j and H/d on Nu_{stag}, and shows the importance of Re_j, i.e., the larger the Re_j,

the higher the Nu_{stag}. While the effect of H/d on the Nu_{stag} under different Re_j were almost the same, and there was an optimal H/d to obtain the maximum Nu_{stag}. With the increase of Re_j, the optimal H/d value decreased slightly, as shown in Table 3. This phenomenon can be theoretically analyzed below. For a given Re_j, when the tube-to-surface distance was smaller than the length of the potential core, the jet arriving at the impinging surface was not fully developed and the central velocity of the jet there would remain unchanged. As H/d decreased, the travelling distance of the jet before arriving at the impinging surface decreased accordingly, and the shear-driven interaction between the jet and the surrounding air was weakened, resulting in the drop of Nu_{stag} due to the decrease of the jet turbulence level at the stagnation point. When the tube-to-surface distance was larger than the length of the potential core, the jet would be fully developed before impinging onto the target surface. Under this condition, the target surface was in the downstream of the jet potential core. As H/d increased, the travelling distance of the jet before arriving at the impinging surface increased accordingly, and the momentum and velocity in the jet core zone would decrease gradually due to the shear-driven interaction between the jet and the surrounding air, resulting in a decrease of the heat transfer performance at the jet impingement stagnation point. Therefore when the tube-to-surface distance was approximately equal to the length of the potential core, the best heat transfer performance at the stagnation point could be obtained. However, the optimal H/d was generally not a fixed value but fell within a range. That was attributed by the tradeoff between an increased jet turbulence due to the interaction with the surrounding air and a decreased jet central velocity. Meanwhile, the length of the potential core would vary with the jet Reynolds number. For example, Gardon and Cobonpue [28] found that the optimal tube-to-surface distance was equal to the length of the potential core to achieve the best heat transfer performance at the stagnation point on a flat plate. Whereas Ashforth-Frost and Jambunathan [29] showed that the optimal tube-to-surface distance was 110% of the length of the potential core for a flat plate. It was because at that H/d position, the effect of turbulence increase on the Nu_{stag} was greater than that of the central velocity loss. In this

paper, the fluid flow and heat transfer of the jet impingement was more complex because the target surface was a variable-curvature concave one in a wing leading edge, and the optimal H/d was found to be within 4 ~ 5.75.

5.2 Effect of jet impingement angle on Nu_{stag}

Fig. 5 shows the influence of the jet impingement angle α on Nu_{stag} with different Re_j at a fixed H/d =10. The jet impingement angle exhibited a significant effect on the heat transfer performance of the jet impingement at the stagnation point. For instance, Nu_{stag} was increased by 47.4% ~ 59.5% when α = 90°, comparing with that when α = 66°. The effect of jet impingement angle was more notable at a larger Re_j. Moreover, the effect of α within 82° ~ 90° on the Nu_{stag} was much stronger compared with that α = 66° ~ 82°. Therefore, when the air jet was changed from a vertical to an oblique jet, the Nu_{stag} would decreased rapidly until α = 82°, after which the attenuation of the Nu_{stag} became much slower.

When the air jet changes from a vertical to an oblique jet, the direction of the jet centerline was no longer perpendicular to the impinging surface at the stagnation point, causing the decrease of the normal velocity component at the stagnation point. The smaller the jet impingement angle, the lower the normal velocity component at the stagnation point, which corresponded to a decreased heat transfer performance at the stagnation point.

5.3 Effect of jet Reynolds number on ξ_x

Fig. 6 shows the distribution of ξ_x in the chordwise direction of the wing leading edge with different Re_j numbers where the curves exhibited a bell shape attenuating from the stagnation point to both sides. The negative-value zone on the abscissa x/d represents the lower surface of the anti-icing cavity, and the positive-value zone represented the upper surface. From Fig. 6 it can be concluded that: 1) the distribution curves of ξ_x at both sides of the stagnation point for three rows of aligned jet holes were obviously different, and the attenuation coefficient dropped more quickly on the lower surface than that on the upper surface. That is mainly caused by the

specific anti-icing cavity structure as shown in Fig. 1, where the only slot for hot air venting was adjacent to the upper surface, and the wall jet along the lower surface was strongly inhibited by the barrier wall. 2) The effect of Re_j on ξ_x in the peak region (x/d=±10) was very small, and the peak regions of the distribution curves of ξ_x corresponding to different Re_j almost overlapped. 3) Re_j obviously affected ξ_x in the non-peak region of the distribution curve, and the larger the Re_j, the faster the attenuation rate of the ξ_x. When Re_j was increased from 51112 to 85340, ξ_x on the lower surface at x/d=-50 decreased by nearly 11%.

5.4 Effect of relative tube-to-surface distance on ξ_x

Fig. 7 shows the distribution of the ξ_x in the chordwise direction of the wing leading edge with different relative tube-to-surface distance H/d. It is observed that the effect of the H/d was very similar to that of Re_j, i.e. the influence of H/d on the ξ_x was very small in the peak region, and it became salient in the non-peak region on the distribution curve. The smaller the H/d, the faster the attenuation rate of ξ_x. When the relative tube-to-surface distance decreased from 13.75 to 6.63, ξ_x value on the lower surface at x/d=-52 dropped by about 8.5%.

5.5 Effect of relative chordwise arc length in the jet impingement zone r/d on ξ_x

Fig. 8 shows the distribution of ξ_x in the chordwise direction of the wing leading edge with different relative arc length r/d. It suggests that the effect of r/d on the ξ_x was much different from those of Re_j and H/d. First, r/d obviously affected ξ_x in the peak region on the distribution curve, and the larger the r/d, the higher the ξ_x in the peak region on the distribution curve. Secondly, r/d also significantly affected ξ_x in the non-peak region. However, on the lower surface of the anti-icing cavity far away from the stagnation point, the effect of r/d on the ξ_x became much weakened compared with those of Re_j and H/d. For instance, when r/d was increased from 16.35 to 34.8, the variation of the ξ_x at x/d= -52 on the lower surface of the anti-icing cavity was within 3.0.

6 Experimental data-based correlation equations

6.1 Correlation of the stagnation Nusselt number

Based on the experimental results, the correlation of the stagnation Nusselt number Nu_{stag} in terms of the jet Reynolds number Re_j, relative tube-to-surface distance H/d and jet impingement angle α_{rad} was obtained as follows:

$$Nu_{stag} = 1.827\times10^{-4} Re_j^{1.124} \alpha_{rad}^{0.847} (H/d)^{-0.487} \quad (5)$$

The above correlation is valid for a wide range of parameters, i.e., 50,000 $\leqslant$ Re_j $\leqslant$ 90,000, 1.74$\leqslant$ H/d $\leqslant$ 20.0, 66°$\leqslant$ $\alpha\leqslant$ 90°, and the average difference between the calculated and experiment results was within 4.0%, as shown in Fig. 9.

6.2 Correlation of the attenuation coefficient

It is of high interest to propose a correlation for the attenuation coefficient ξ_x, to obtain quickly and accurately the distribution characteristics of the jet impingement heat transfer in the chordwise direction if the correlation of the stagnation Nusslet number is available. For the structure of three rows of aligned jet holes, the correlation of ξ_x in terms of three dimensionless parameters Re_j, H/d and r/d was established. As explained above, the ξ_x～x/d curve exhibited an approximate bell shape attenuating from the stagnation point to both sides along the upper and lower surfaces of the anti-icing cavity. To neglect the effect of the slot structure on the heat transfer on the upper surface, which made this issue much more complex, and on a basis of conservative design, the ξ_x～x/d curve on the upper surface was replaced by the one on the lower surface, thus forming a strictly symmetrical and bell-shaped curve of ξ_x. The Gauss function expressed by Equation (6) was applied to fit the experimental data of ξ_x.

$$\xi_x = \xi_0 + \frac{A}{w\sqrt{\pi/2}} e^{-2\frac{(x/d - x_{stag}/d)^2}{w^2}} \quad (6)$$

where ξ_0 is the value of ξ_x at the farthest position from the stagnation point; x_{stag} is the coordinate of the stagnation point whose value is zero in the paper; $A/w\sqrt{\pi/2}$ is the attenuation height H_a, which is equal to ξ_{stag}-ξ_0; ξ_{stag} is the value of ξ_x at the stagnation point whose value is 100 in this paper; w is $1/\sqrt{\ln 4}$ times of the Gauss fitted

curve width at the half of the attenuation height $H_a/2$.

The attenuation coefficient M is defined as $M = 2/w^2$ and Equation (7) was derived from Equation (6) as follows:

$$\xi_x = (\xi_{stag} - H) + H \times e^{-M(x/d - x_{stag}/d)^2} = (100 - \pi^{-0.5} AM^{0.5}) + \pi^{-0.5} AM^{0.5} e^{-M(x/d)^2} \quad (7)$$

According to Equation (7), non-linear fitting technique was applied to fit the experimental data samples, each of which yielded a certain A and M value, with the fitting correlation factor, R, ranging from 0.980 to 0.996. Further analysis indicated that both M and A in Equation (7) were strong functions of Re_j, H/d and r/d. As shown in Fig. 10, the unary effects of Re_j, H/d and r/d on both M and A exhibited approximate exponential relationship, so exponential functions were applied to fit M and A, respectively, in terms of Re_j, H/d and r/d, as shown in Equations (8) and (9), and the correlation factors were 0.96 and 0.98, respectively.

$$M = 0.009385 Re_j^{0.4970} (H/d)^{-0.1320} (r/d)^{-2.1134} \quad (8)$$

$$A = 14.0566 Re_j^{0.1512} (H/d)^{-0.1331} (r/d)^{1.1095} \quad (9)$$

Substituting Equations (8) and (9) into Equation (7), Equation (10) was derived, which was applicable in the following parameter ranges: $5.0\times10^4 \leqslant Re_j \leqslant 9\times10^4$, $1.74 \leqslant H/d \leqslant 20.0$ and $13.2 \leqslant r/d \leqslant 34.8$.

$$\begin{aligned}\xi_x = {} & 100 - 0.76828 Re_j^{0.39970} (H/d)^{-0.19912} (r/d)^{0.052781} + \left[0.76828 Re_j^{0.39970} (H/d)^{-0.19912} (r/d)^{0.052781}\right] \times \\ & \exp\left[-0.009385 Re_j^{0.4970} (H/d)^{-0.1320} (r/d)^{-2.1134} (x/d)^2\right]\end{aligned} \quad (10)$$

To validate the correlation of ξ_x, a comparison between the experimental data including both the sample and non-sample data and the calculation results based on the correlation equation was conducted, as presented in Fig. 11. The deviations between the experiment data and the calculation results from the correlation were all lower than 2.4%, indicating that the correlation was effective within the proposed parameter range. For this specific structure, the correlation can accurately predict the distribution characteristics of the jet impingement heat transfer in the chordwise direction on the surface of the anti-icing cavity, which is of great use to guide the design and performance assessment for a wing leading edge hot-air anti-icing system.

7 Conclusions

Extensive experimental studies of the heat transfer characteristics of jet impingement on a variable-curvature concave surface in a wing leading edge were conducted in this work, which can be summarized as follows:

- The Re_j and H/d exhibited significant effects on the jet impingement heat transfer performance at the stagnation point. The larger the Re_j, the higher the heat transfer performance, and there existed an optimal H/d corresponding to the maximum Nu_{stag}. For the experimental conditions in this work, the optimal H/d was in the range of 4 ~ 5.75 with the structure of three rows of aligned jet holes on the piccolo tube.
- Increasing jet impingement angle (α) can enhance the jet impingement heat transfer performance at the stagnation point. It was found that the Nu_{stag} decreased much faster with the decrease of the jet impingement angle when $82° \leqslant \alpha \leqslant 90°$ than that when $66° \leqslant \alpha \leqslant 82°$.
- The distribution curve of the attenuation coefficient in the chordwise direction exhibited a bell shape. In the peak region of the distribution curve, the attenuation coefficient was mainly affected by r/d, and the larger the r/d, the higher the ξ_x in the peak region; while in the non-peak region, it was significantly affected by Re_j, H/d and r/d.
- Based on the experimental data, correlations of the stagnation Nusselt number (Nu_{stag}) and the distribution of the attenuation coefficient (ξ_x) in the chordwise direction were developed and validated, which are applicable to the following parameter ranges: $5.0 \times 10^4 \leqslant Re_j \leqslant 9 \times 10^4$, $1.736 \leqslant H/d \leqslant 20.0$, $66° \leqslant \alpha \leqslant 90°$ and $13.21 \leqslant r/d \leqslant 34.8$.

As the piccolo tube-based anti-icing cavity design is well adopted by many aircraft engineers, especially for the piccolo tube with two or three rows of jet holes, this work is of great help to the design and performance evaluation of the aircraft wing leading-edge anti-icing system.

Acknowledgement

This work was supported by the National Natural Science Foundation of China (Grant No. 51206008) and the EU Marie Curie Actions-International Incoming Fellowships (FP7-PEOPLE-2013-IIF-626576). The authors would like to express our gratitude to Ying Zhou and Lu Xin from the Laboratory of Fundamental Science on Ergonomics and Environmental Control, Beihang University, for their help during the experiments.

References

[1] T. S. O'Donovan, D. B. Murray, Jet impingement heat transfer - Part I: Mean and root-mean-square heat transfer and velocity distributions, Int. J. Heat Mass Transfer 50 (2007) 3291-3301

[2] T. S. O'Donovan, D. B. Murray, Fluctuating fluid flow and heat transfer of an obliquely impinging air jet, Int. J. Heat Mass Transfer 51 (2008) 6169-6179

[3] D.H. Lee, Y.S. Chung, S.Y. Won, The effect of concave surface curvature on heat transfer from a fully developed round impinging jet, Int. J. Heat Mass Transfer 42(1999) 2489-2497

[4] D. Lytle, B. W. Webb, Air jet impingement heat transfer at low nozzle-plate spacings, Int. J. Heat Mass Transfer 37 (1994) 1687-1697

[5] G.M. Carlomagno, A. Ianiro, Thermo-fluid-dynamics of submerged jets impinging at short nozzle-to-plate distance: A review, Experimental Thermal and Fluid Science 58(2014) 15-35

[6] E. Öztekin, O. Aydin, M. Avcı, Hydrodynamics of a turbulent slot jet flow impinging on a concave surface, Int. Commun. Heat Mass Transfer 39 (2012) 1631-1638

[7] G. Yang, M. Choi, J. S. Lee, An experimental study of slot jet impingement cooling on concave surface: effects of nozzle configuration and curvature, Int. J. Heat Mass Transfer 42 (1999) 2199-2209

[8] E. Öztekin, O. Aydin, M. Avcı, Heat transfer in a turbulent slot jet flow impinging on concave surfaces, Int. Commun. Heat Mass Transfer 44 (2013) 77-82

[9] X. Yan, N. Saniei, Heat transfer from an obliquely impinging circular, air jet to a flat plate, Int. J. Heat Flui Flow 18 (1997) 591-599

[10] M. Attalla, M. Salem, Experimental investigation of heat transfer for a jet impinging obliquely on a flat surface, Exp. Heat Transfer 28 (2015) 378-391

[11] C. Meola, L. de Luca, G.M. Carlomagno, Influence of shear layer dynamics on impingement heat transfer, Exp. Therm. Fluid

Sci. 13 (1996) 29-37

[12] C. Cornaro, A. S. Fleischer, R. J. Goldstein, Flow visualization of a round jet impinging on cylindrical surfaces, Exp. Therm. Fluid Sci. 20 (1999) 66-78

[13] M. Fenot, E. Dorignac, J.-J. Vullierme, An experimental study on hot round jets impinging a concave surface, Int. J. Heat Fluid Flow 29 (2008) 945-956

[14] P. Planquart, G.V. Borre, J.M. Buchlin, Experimental and numerical optimization of a wing leading edge hot air anti-icing system, AIAA paper 2005-1277, 2005.

[15] V.J. Jusionis, Heat transfer from impinging gas jets on an enclosed concave surface, J. Aircraft, 7 (1) (1970) 87-88.

[16] J. M. Brown, S. Raghunathan, J.K. Watterson, et al., Heat transfer correlation for anti-icing systems. J. Aircraft 39(1) (2002) 65-70.

[17] W.B. Wright, An evaluation of jet impingement heat transfer correlations for piccolo tube application, AIAA paper 2004-62, 2004.

[18] R. J. Goldstein, A. I. Behbahani, K. Heppelmann, Streamwise distribution of the recovery factor and the local heat transfer coefficient to an impinging circular air jet, Int. J. Heat Mass Transfer 29 (1986) 1227-1235.

[19] M. Fregeau, F. Saeed and I. Paraschivoiu, Numerical heat transfer correlation for array of hot-air jets impinging on 3-dimensional concave surface, J. Aircraft 42(3) (2005) 665-670.

[20] F. Saeed, Numerical simulation of surface heat transfer from an array of hot-air jets, J. Aircraft 45(2) (2008) 700-714.

[21] M. Fregeau, M. Gabr, I. Paraschivoiu and F. Saeed, Simulation of heat transfer from hot-air jets impinging a three-dimensional concave surface, J. Aircraft 46(2) (2009) 721-725.

[22] M. Papadakis, S.J. Wong, Parametric investigation of a bleed air ice protection system, AIAA paper 2006-1013, 2006.

[23] M. Papadakis, S.J. Wong, H.W. Yeong, et al., Icing tunnel experiments with a hot air anti-icing system, AIAA paper 2008-444, 2008.

[24] M. Papadakis, S.J. Wong, H.W. Yeong, et al., Icing tests of a wing model with a hot-air ice protection system, AIAA Paper 2010-7833, 2010.

[25] M. Imbriale, A. Ianiro, C. Meola, et al., Convective heat transfer by a row of jets impinging on a concave surface. Int. J. Therm. Sci. 75(2014) 153-163.

[26] C. Meola, A new correlation of Nusselt number for impinging jets, Heat Transfer Eng. 30(3) (2009) 221-228.

[27] X. Bu, L. Peng, G. Lin, L. Bai, et al., Experimental study of jet impingement heat transfer on a variable-curvature concave surface in a wing leading edge, Int. J. Heat Mass Transfer 90 (2015) 92-101.

[28] R. Gardon, J. Cobonpue, Heat transfer between a flat plate and jets of air impinging on it, Int. Heat Transfer Conf. Pt. 2 (1961) 454-460.

[29] S. Ashforth-Frost, K. Jambunathan, Effect of nozzle geometry and semi-confinement on the potential core of a turbulent axisymmetric free jet, Int. Commun. Heat Mass Transfer 23 (1996) 155-162.

Nomenclature

A	attenuation coefficient
C_n	spanwise distance between adjacent jet holes, m
c_p	pressure coefficient
d	jet hole diameter, m
G_m	Mass flowrate, g/s
h_x	local convective heat transfer coefficient, $W/(m^2 \cdot K)$
H	piccolo tube-to-surface distance, m;
H_a	attenuation height
M	attenuation coefficient
N	number of jet holes
Nu_x	local Nusselt number
Nu_{stag}	stagnation Nusselt number
q	heat flux, W/m^2
r	arc length between jet stagnation points, mm
Re_j	jet Reynolds number
T_{in}	supplied air temperature, K
T_{wx}	local temperature on the internal surface of the wall, K

Greek symbols

α	jet impingement angle (°)
ρ	density, kg/m^3
θ	circumferential angle of jet holes on the piccolo tube (°)

λ	thermal conductivity, W/(m · K)
v	kinetic viscosity, m^2/s
μ	dynamic viscosity, Pa·s
ξ_x	attenuation coefficient of Nu, Nu_x/Nu_{stag}

Table captions

Table 1 Parameter range in the experiments

Table 2 Uncertainties of measuring equipments

Table 3 The maximum Nu_{stag} at corresponding H/d under different Re_j

Figure captions

Table 1 Parameter range in the experiments

Parameters	Range
C_n (mm)	50
d (mm)	2
H/d	1.74 ~ 20.0
r/d	13.2 ~ 34.8
α	66° ~ 90°
Re_j	50000 ~ 90000

Table 2 Uncertainties of measuring equipments

Equipment	Accuracy grade	Measuring error
T Type thermocouple	I	±0.004|T|
PT100 thermal resistance	II	±(0.30±0.005|T|)
Pressure transmitter	II	±0.2%F.S
Standard 24-volt outlet	II	0.2%
air mass flow meter	II	±0.2%F.S

Table 3 The maximum Nu_{stag} at corresponding H/d under different Re_j

Re_j	Optimal Nu_{stag}	Corresponding H/d
51341	26	5.6
68775	42.9	4.5
76668	47.5	4.2
85797	62.5	4.1
99296	72	4.0

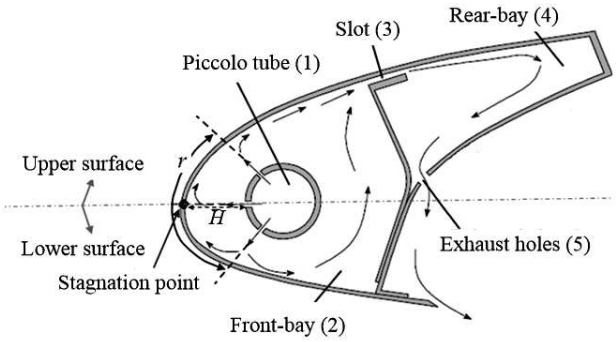

Fig. 1 Schematic of a typical wing leading edge hot-air anti-icing cavity

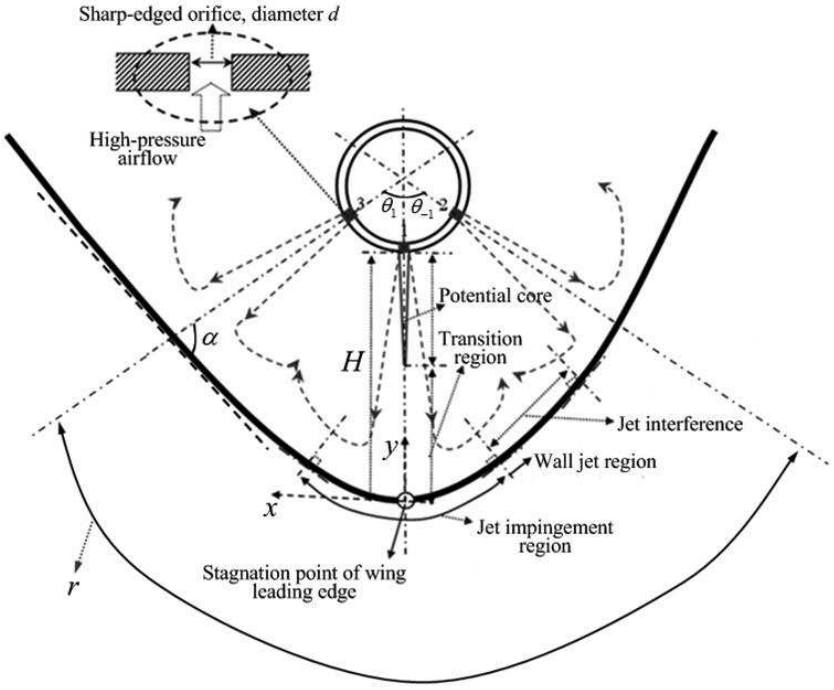

Fig. 2 Schematic of jet impingement on a concave surface from a piccolo tube

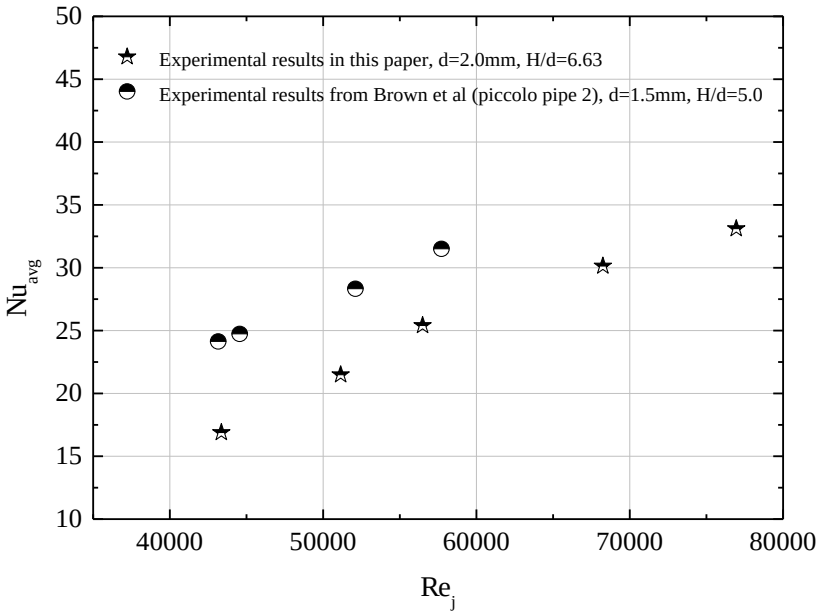

Fig. 3 Comparison and validation of the experimental results

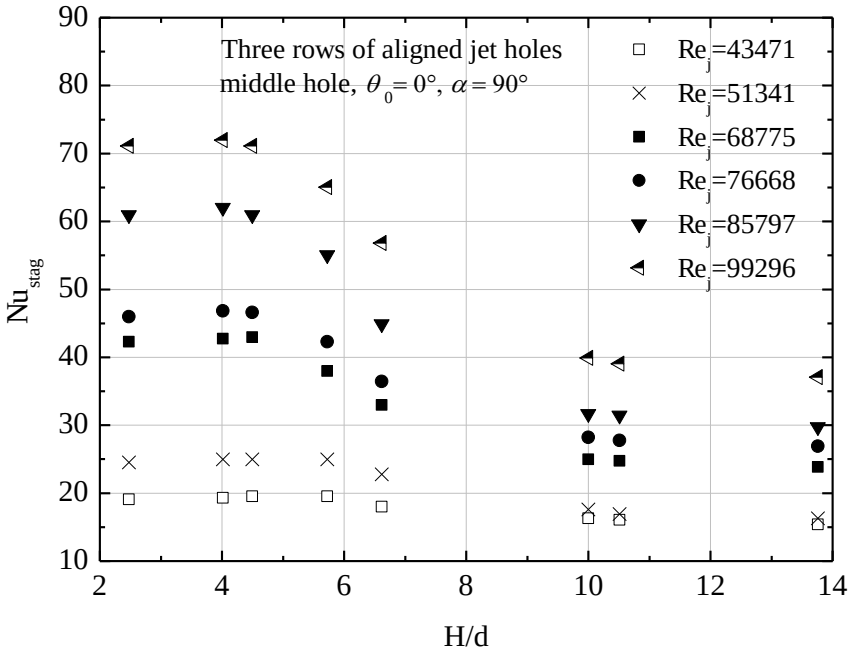

Fig. 4 Influence of relative tube-to-surface distance on Nu_{stag}

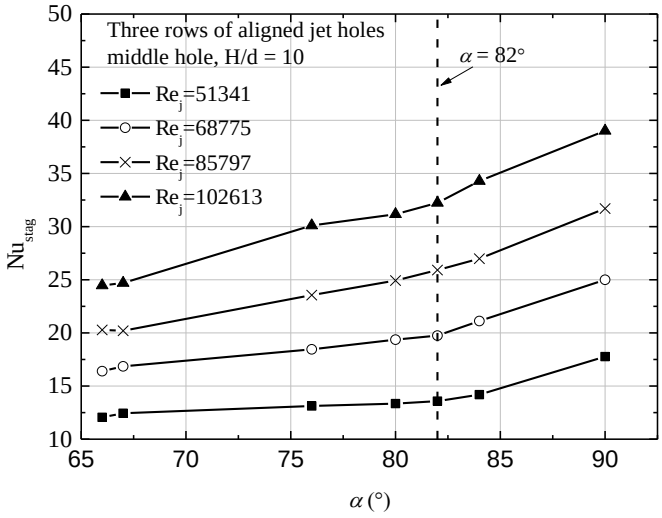

Fig. 5 Influence of jet impingement angle on Nu_{stag}

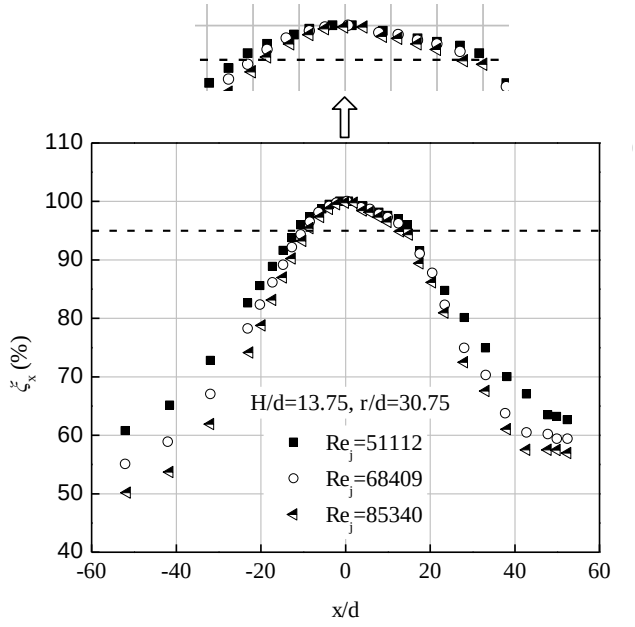

Fig. 6 Influence of Re_j on the ξ_x distribution in the chordwise direction

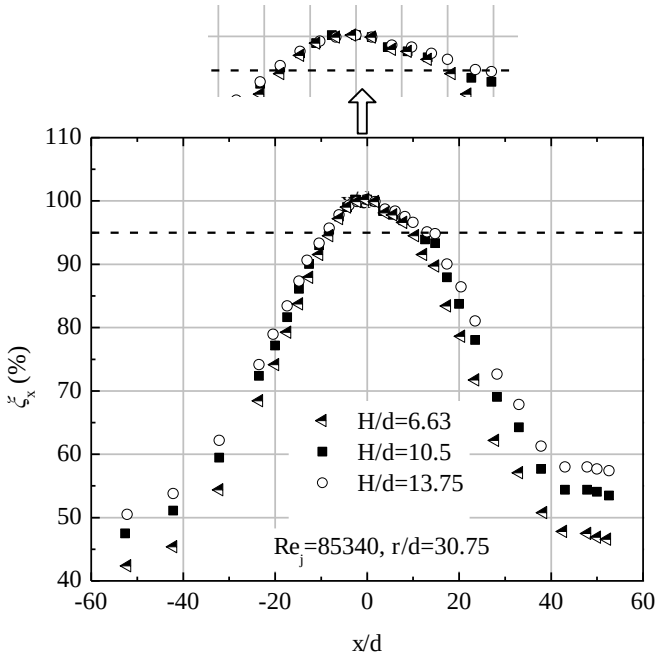

Fig. 7 Influence of H/d on the ξ_x distribution in the chordwise direction

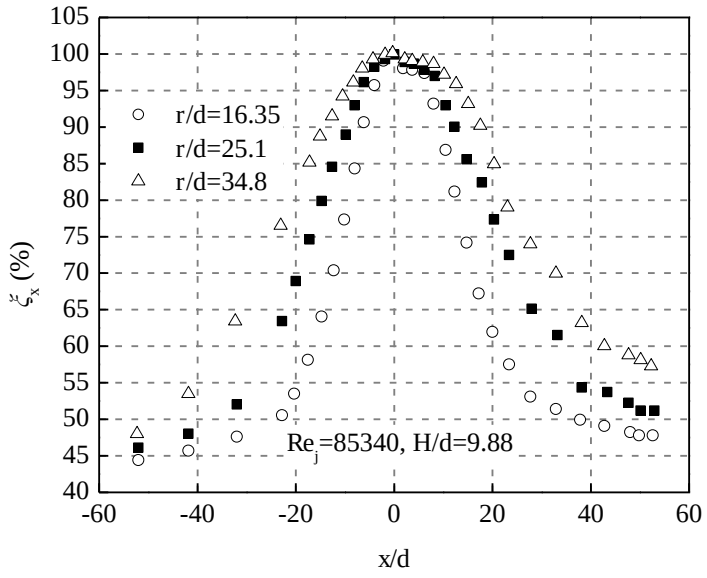

Fig. 8 Influence of r/d on the ξ_x distribution in the chordwise direction

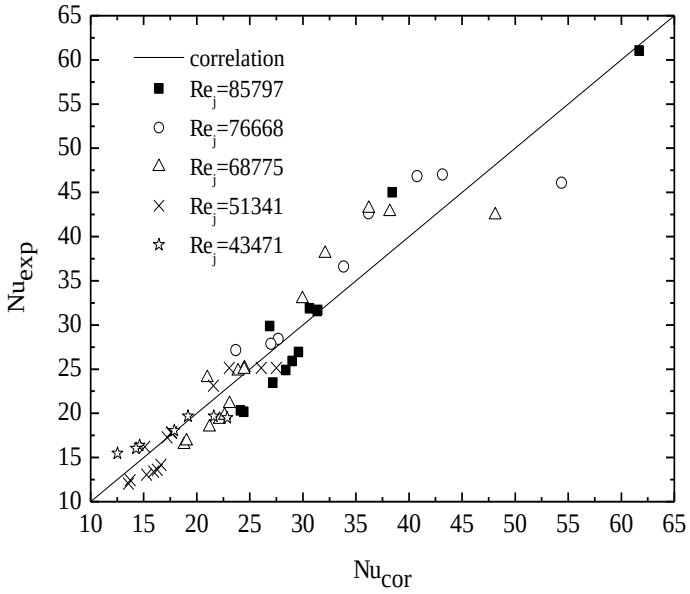

Fig. 9 Comparison between calculated and experimental results for stagnation Nusselt number

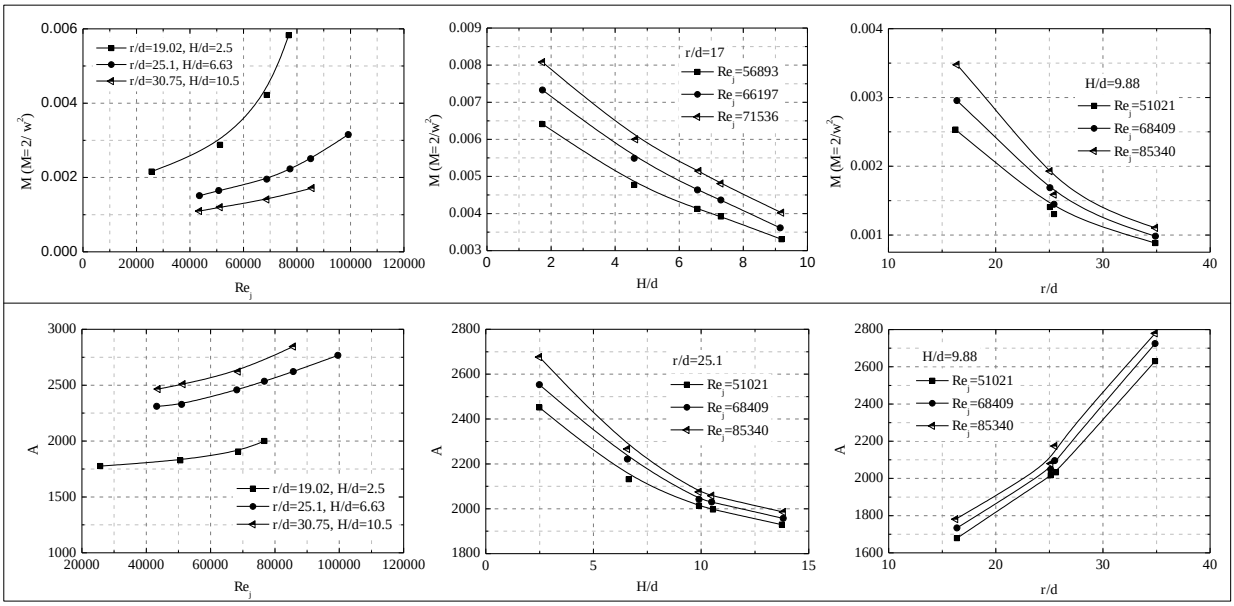

Fig. 10 Fitted curves of M and A in terms of Re_j、H/d and r/d

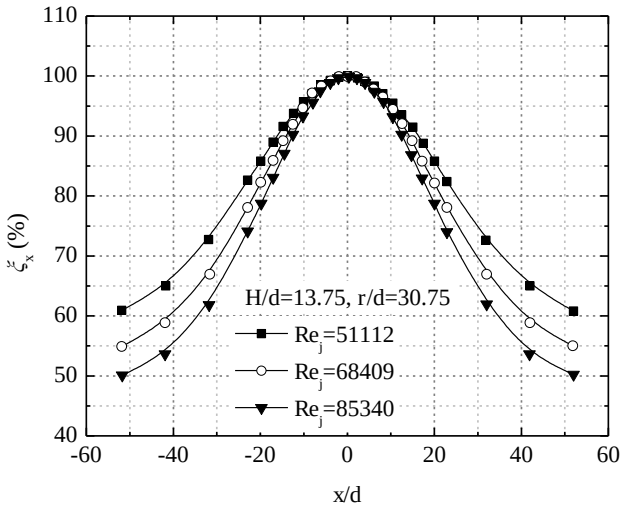

(a) sample experimental data

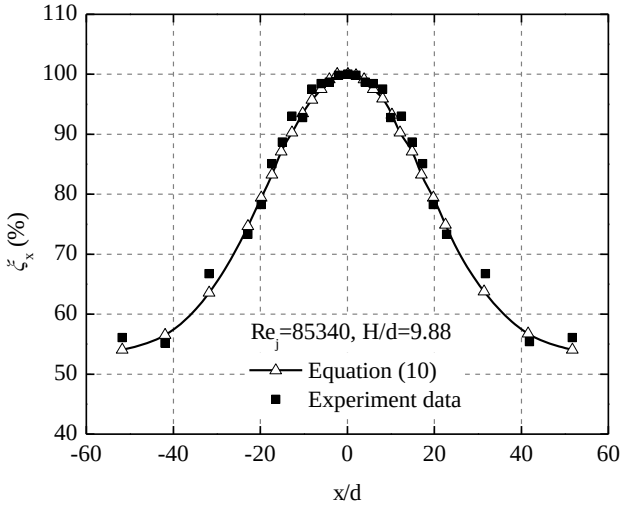

(b) non-sample experimental data

Fig. 11 Comparison of results from the experiments and correlation equation for ξ_x